Hartree-Fock study of lithium hydride with the use of a polarizable basis set

R. Dovesi, C. Ermondi, E. Ferrero, C. Pisani, and C. Roetti
Institute of Theoretical Chemistry, University of Torino, Via P. Giuria 5, I-10125 Torino, Italy
(Received 8 August 1983)

Crystalline LiH is studied at a linear combination of atomic orbitals—Hartree-Fock level of approximation with the use of two basis sets: a minimal basis set comprising a single Slater-type orbital per atom (minimal closed-shell model), and an extended set comprising 11 independent *s*- and *p*-type atomic orbitals per unit cell (extended-basis-set model). The problem of an adequate treatment of long-range Coulomb interactions (which is of great importance with polarizable ionic systems) has been solved by including a Madelung potential in the Fock operator. Cohesive energy, bulk modulus, band structure, x-ray structure factors, and electron-momentum distribution data are calculated and discussed. The agreement with experiment is in general very good with the extended-basis-set model. The present study confirms the essentially ionic nature of LiH.

I. INTRODUCTION

The Hartree-Fock (HF) approach is believed to provide an accurate description of ionic crystals since most systematic errors due to correlation effects cancel when subtracting the corresponding free-ion term.[1] A reasonable approximation to the HF solution of these crystals can be constructed within a crystalline orbital-LCAO formalism using a minimal set of atomic orbitals (AO's) able to describe the individual ions; in order to account for the deformation of the AO's in the field of the crystal, scale factors can be used as variational parameters. No self-consistency problem is left since for each reciprocal-space vector $\vec{k}$, the density matrix $P(\vec{k})$ is simply the inverse of the overlap matrix $S(\vec{k})$. This model is sometimes called the "minimal-closed-shell" model (MCS). Its application is particularly simple in the case of lithium hydride because only two AO's are there needed to accommodate the four electrons associated with each crystal cell. For this reason a number of theoretical MCS calculations have been performed for LiH in past and recent years[2–16] (for a rather detailed discussion of theoretical work up to 1977, see Ref. 17). For a long time, before the advent of powerful computers, one of the main problems has been the accurate evaluation of the inverse-overlap matrix. It has recently been recognized that due to the large size of the H^- ion, a large number of neighbors must be taken into consideration[11,12] and that many of the less recent calculations suffer seriously from lack of orthogonality of the crystalline orbitals. The second main problem has been the choice of an adequate function χ_H to describe the hydride ion. With few exceptions (Kunz[6] modeled, for instance, the radial dependence of χ_H by approximately taking into account the crystal field according to the Adams-Gilbert method), a 1*s* Slater-type orbital (STO) has generally been used for χ_H, with a suitable scale factor α_H; values of α_H ranging from 0.6875 (free-ion value) to 0.837 a.u. have been proposed. The ionic model just described provided a reasonable explanation of some essential physical properties of LiH: cohesive energy,[3] x-ray structure factors,[15] and Compton profiles (CP's).[16]

On the other hand, the limits of this simplified description have been recognized from early years[3] and are essentially related to the high polarizability of H^-. Kunz[6] has shown that the radial behavior of χ_H must differ appreciably from 1*s* STO's in order to account for crystal-field effects. Besides, an analysis[17] of the CP's has shown that the electron-momentum distribution (EMD) of LiH cannot be explained without introducing an anisotropy of the valence Wannier function which goes beyond orthogonality effects. Both these requirements of a richer radial and angular description of the wave function can be met, in principle, using a reasonably extended basis set. It is the purpose of the present paper to perform such a calculation (to be referred to in the following as "extended basis set," or EBS) and to compare the corresponding results with those obtained using an MCS model. The resulting information can be precious for the interpretation of the structure of H^- in alkali hydrides and other ionic hydrides. The use of EBS's has been suggested for a proper description of more general classes of ionic crystals,[18] and it appears nearly mandatory when studying the reaction properties of their surfaces using, for instance, a thin-film model.

The present calculation represents a severe test of the computational techniques adopted in the CRYSTAL program[19,20] used in the past for the solution of the HF problem. In fact, defining a self-consistent wave function becomes a delicate problem in the presence of long-range Coulomb terms with a system that is purposedly described as highly polarizable. This problem is dealt with in Sec. II. It is shown that the neglect of the electrostatic potential contributed by crystal cells beyond a certain distance in the construction of the Fock matrix causes large errors in the present case. The simple technique that has been adopted for including electrostatic interactions up to infinite distance is also described. In Sec. III the choice of the minimal basis sets and EBS's that have been used for the present calculations is first justified, then the results are presented and discussed. The results concern total and

 ©1984 The American Physical Society

cohesive-energy data, bulk modulus, band structure, charge density, and EMD. Particular attention is devoted to the distribution of momenta, since there is very rich and reliable experimental information resulting from directional CP's.

II. MADELUNG POTENTIAL

We have recently performed a detailed analysis of the problem of the correct evaluation of Coulomb terms in HF calculations of periodic systems, and described the way it is handled in the CRYSTAL program.[20] Essentially our procedure is as follows: (a) The interaction of two charge distributions contributing to the total charge in cells $\vec{0}$ and $\vec{m}$ is treated exactly at short range; (b) when the reciprocal penetration of the distributions is sufficiently small, the electronic charge in cell $\vec{m}$ is partitioned into "shell-charge distributions" which are then expanded in a multipole series; (c) for $|\vec{m}|$ larger than a given radius M (the Madelung radius), the multipole series is truncated to the first (charge) term; the effect of the atomic charges beyond M is included in the energy expression as a classical Madelung term, but is altogether ignored in the Fock operator. The above-described technique has been shown to work very well with a number of different systems (metals, insulators, semiconductors, thin films, and polymers) with little or no ionic character. We have already pointed out that in the case of ionic crystals, especially three-dimensional ones,[21] rather large Madelung effects on the wave function were to be expected. Suppose, in fact, that a certain radius M has been fixed, and we indicate as Madelung potential, or $V^{\mathrm{Mad}}(\vec{r})$, the electrostatic potential contributed at a given point $\vec{r}$ within the sphere of radius M by the charge distributions associated with all the cells centered outside the sphere. If V^{Mad} is neglected in the construction of the Fock matrix, the latter can be wrongly calculated because of an artificial field which sets in inside the sphere due to the presence of free charges of opposite sign at the two ends of the sphere in the direction of the cell dipole. In particular, the element $F_{\mu\nu}^{\vec{0}\,\vec{n}}$, which relates the AO's χ_μ and χ_ν in cells $\vec{0}$ and $\vec{n}$, respectively, will differ from $F_{\nu\mu}^{\vec{0}-\vec{n}}$, thus destroying the hermiticity of $F(\vec{k})$. The entity of this error obviously depends on the magnitude of the variation of V^{Mad} in the zone spanned by the product distributions $\chi_\mu^{\vec{0}}\chi_\nu^{\vec{n}}$. Suppose the unit cell of LiH is chosen to contain third-neighbor lithium and hydrogen atoms, with hydrogen at the origin and lithium along the [111] direction, and $M=18.1$ a.u., corresponding to the inclusion of twelve full stars of cells within the sphere. Then, within few a.u. from the center of the sphere, the linear relation $V^{\mathrm{Mad}}(x,y,z)=-0.27+0.0491(x+y+z)$ is observed to hold with very good approximation (both the potential and the lengths are expressed in a.u.). It is clear that neglecting a term which depends so strongly on position causes deep effects on the wave function if the polarizability of H^- is accounted for by an EBS. Consider, for instance, the first two columns of Table I, which report the results of two calculations performed with an EBS (to be described in the next section), setting $V^{\mathrm{Mad}}=0$ and using two different choices of the unit cell (containing first- and third-neighbor lithium and hydrogen atoms, respectively). Far from coinciding, the two results reflect in an impressive way the different importance of the V^{Mad} term in the two cases. Note that the corresponding calculations performed with a minimal basis set do coincide, due to the lack of variational freedom, and thus give much more reasonable results: The total energy is -8.010 a.u., and the kinetic energy is 8.082 a.u. Taking into account the effect of the Madelung potential on the general element $F_{\mu\nu}^{\vec{0}\,\vec{n}}$ of the Fock matrix is simple enough if we assume the linearity of V^{Mad} over the region where the overlap density $\chi_\mu(\vec{r})\chi_\nu(\vec{r}-\vec{n})$ differs appreciably from zero,

$$\langle\chi_\mu^{\vec{0}}\,|\,V^{\mathrm{Mad}}\,|\,\chi_\nu^{\vec{n}}\rangle\simeq SV^{\mathrm{Mad}}(\vec{c})+\vec{\gamma}_{\vec{c}}\cdot\mathrm{grad}[V^{\mathrm{Mad}}(\vec{c})]\,. \quad (1)$$

Here S is the overlap integral $\langle\chi_\mu^{\vec{0}}\,|\,\chi_\nu^{\vec{n}}\rangle$ and $\vec{c}$ is a suitable center with respect to which the dipole moment of the distribution is evaluated; we have taken $\vec{c}$ to coincide with the center of gravity of the two adjoined Gaussians associated with the two AO's.[20] For calculating V^{Mad} and its gradient at a specific position, we have assumed that the charge distributions in the cells outside the sphere can be approximated by a multipole expansion truncated at the first (charge-only) level. The classical expression for the Madelung potential $V_{\mathrm{tot}}^{\mathrm{Mad}}$ (Refs. 22–24) can then be used. The inclusion of V^{Mad} in the Fock operator not only reestablishes the hermiticity of $F(\vec{k})$, but also makes the

TABLE I. Effect of the Madelung potential on the results for LiH. The calculations were performed using an EBS (see Table II) with two different choices of the unit cell, containing first-neighbor Li and H atoms or third-neighbor atoms. With reference to Eq. (1), three levels of approximation were considered in the treatment of the Madelung-potential contribution to the Fock matrix elements: (i) full neglect of V^{Mad}, (ii) use of $V^{\mathrm{Mad}}(\vec{c})$ but neglect of $\mathrm{grad}V^{\mathrm{Mad}}(\vec{c})$, and (iii) inclusion of both terms as in Eq. (1). In all cases the Madelung correction was included in the total-energy expression. All units are a.u.

Approximation for V^{Mad}	Complete neglect		Neglect of gradient		As in Eq. (1)	
Unit cell	First neighbor	Third neighbor	First neighbor	Third neighbor	First neighbor	Third neighbor
Total energy	−7.964 582	−7.721 480	−8.060 622	−8.055 382	−8.062 888	−8.062 890
Kinetic energy	8.181 625	8.366 291	8.063 766	8.049 010	8.067 730	8.067 730
Madelung energy	−0.162 745	−0.184 829	−0.262 709	−0.683 054	−0.263 333	−0.687 245
Mulliken net charge on Li	0.78	0.38	0.98	0.97	0.98	0.98

results totally insensitive to the choice of the unit cell, as in the last two columns of Table I. From the data reported in the two central columns of Table I, it is seen that in the present case the inclusion of the gradient term in Eq. (1) does not matter very much. This is because with our choice of $\vec{c}$ it is easily seen that $\vec{\gamma}_{\vec{c}}$ is approximately zero for all distributions involving s orbitals. This is no longer true for s-p distributions, which, however, do not contribute appreciably to the ground state of LiH.

III. RESULTS AND DISCUSSION

A. Computational conditions

Table II reports the basis sets employed for the present MCS and EBS calculations; in both cases nGTO variational functions have been used, i.e., linear combinations of n Gaussian-type orbitals (GTO's). The two MCS functions are 4GTO best-fit approximations to the $1s$ STO,[25] with $\alpha=2.6875$ and 0.772 42 for Li^+ and H^-, respectively. These are the optimum values obtained by Hurst[26] for the individual ions with a model Hamiltonian where point charges approximated the crystal field about the ion; they have since been used by many authors.[7,12,14] While our own calculations have indicated that the optimum α_H value is somewhat higher (around 0.81 a.u.), we have preferred to use the more standard scale factor to make comparisons easier, and also because the various calculated quantities do not change very much in that narrow range of α values.[12,17] The EBS has been chosen after many calculations. A very rich set of independent s functions was first explored in order to fix the coefficients of the high-exponent Gaussians which describe the wave function near the nuclei. The exponents of the outer s functions were then chosen so as to allow adequate variational freedom and efficiency. The effect of the inclusion of a shell of p-type GTO's centered on hydrogen and lithium has finally been considered. In the cases of H and Li a minimum in total energy was found with exponent coefficients of 0.3 and 0.6 a.u., with an energy gain of 0.002 and 0.003 a.u., corresponding to a p population of 0.006 and 0.028 electrons, respectively. In this optimization we had no linear-dependency problems of the kind encountered with metallic lithium.[27]

The calculations to be discussed in the following were performed by fixing the computational parameters so as to insure a numerical accuracy better than 10^{-3} a.u. in total energy. In particular, the t_2 parameter which fixes the penetration threshold of two charge distributions, beyond which the Coulomb interactions are treated exactly, has been fixed to 10^{-3}. The Madelung radius (see Sec. II) has been assigned a value of 18.1 a.u., exchange sums have been limited to within four stars of neighboring cells,[19] and no multipole terms have been used in the evaluation of Coulomb interactions between separate distributions, after having verified that inclusion of hexadecapoles (lowest nonzero multipoles) contributed to the total energy by only $+2.5\times10^{-5}$ a.u. In all cases, except when calcu-

TABLE II. Exponents (in a.u.) and coefficients of the s and p Gaussian functions used in the present MCS and EBS calculations. The contraction coefficients multiply normalized individual s and p Gaussians.

Model	Function number	Center	Type	Exponent	Coefficient
MCS	1	H	s	4.315 640	0.026 136
				0.763 489	0.135 792
				0.197 838	0.353 250
				0.060 341	0.259 239
	2	Li	s	52.246 5	0.169 629
				9.243 05	0.881 319
				2.395 09	2.292 67
				0.730 507	1.682 52
EBS	1	H	s	120.0	0.000 267
				40.0	0.002 249
				12.0	0.006 389
				4.0	0.032 906
				1.2	0.095 512
	2	H	s	0.5	1.0
	3	H	s	0.13	1.0
	4–6	H	p	0.3	1.0
	7	Li	s	700.0	0.001 421
				220.0	0.003 973
				70.0	0.016 390
				20.0	0.089 954
				5.0	0.315 646
				1.5	0.494 595
	8	Li	s	0.5	1.0
	9–11	Li	p	0.6	1.0

lating the bulk modulus, the experimental geometry of the fcc crystal was adopted, corresponding to a nearest-neighbor distance of 3.858 a.u.

B. General features of the solutions

Table III summarizes some results of the two calculations. It is seen that the EBS model brings in an appreciable increase in stability and a net improvement of the virial coefficient. The cohesive energy has been calculated by subtracting the HF energy of the free ions from the total energy per unit cell.[28] The EBS result is close to the experimental value of 0.346 a.u.,[3,29] but the MCS model also accounts for the largest portion of the cohesive energy, thereby confirming early results[3]: A further 3×10^{-3} a.u. can be gained within the MCS model if the optimum scale factor $\alpha_H=0.81$ a.u. is used. For the EBS model we explored the dependence of total energy on the nearest-neighbor distance r_0. The basis set was the same as in Table II except for the exponent on the outermost p and s GTO's on hydrogen, which was varied proportionally to $1/r_0^2$, following a suggestion by Surratt *et al.*[30] As usual in HF calculations, the energy minimum corresponded to a slightly expanded structure ($r_0=3.876$ a.u. as opposed to the observed value of 3.858 a.u.) with an energy gain of only 0.000 11 a.u. The EBS bulk modulus, obtained from $d^2E/(dr_0)^2$, was in the range of the experimental uncertainty [$2.28-3.47\times10^{11}$ dyn/cm^2 (Ref. 29)].

Also in Table III the valence-band eigenvalues at the special $\vec{k}$ points are reported. The MCS and EBS bands differ appreciably; in particular, the valence-band widths are 0.276 and 0.245 in the two cases. It is of some interest to compare the present band-structure results with those obtained by Grosso and Pastori Parravicini,[31] who described the core and valence states with an MCS model, but ignored orthogonality effects, and used an orthogonalized-plane-wave treatment for the conduction bands. Their valence-band width (0.478 a.u.) is nearly twice as large as the present MCS and EBS ones, and the shape of their valence band is more similar to the EBS than to the MCS one. Such results are not easily explained, except perhaps by considering their use of a very contracted hydrogen orbital ($\alpha_H=1.050$ a.u.). If the first virtual band is considered in the EBS case, it is found that the direct gaps at Γ and X are 1.27 and 0.49 a.u., respectively, to be compared with Grosso's values of 1.38 and 0.34 a.u.; the introduction of the p orbitals on hydrogen turned out to be essential for a proper description of the first conduction band, particularly at X. Obviously, correlation corrections have very deep effects on calculated gaps and bandwidths. For example, Kunz and Mickish[10] have shown that the direct gap at X was reduced from 0.55 a.u., as resulting from their HF MBS calculation, to 0.23 a.u. after correlation was roughly taken into account according to an electronic polaron model.

C. Electron charge distribution

Experimental x-ray structure factors provide, in principle, the means for checking the accuracy of the calculated charge density. In the case of LiH, reference is usually made to the set of diffraction data produced by Calder *et al.* over 20 years ago;[32] there the intensities of 21 reflections are reported, together with an accurate analysis of experimental errors and an ample comparison with available theoretical data.[3–5,26] A major problem when comparing theoretical and experimental structure factors is accounting for thermal motion, which is particularly important for light atoms such as lithium and hydrogen. An obvious choice with an MCS treatment of ionic systems is to assume that the electrons belonging to a given ion are rigidly following the motion of the corresponding nucleus. The thermal effects are then accounted for by applying to each ion a Debye-Waller correction with a suitable B factor; reference can here be made to the values B_{Li} and B_H measured by Calder[32] using x-ray and neutron diffraction. For the EBS model we proceeded analogously, by applying a Debye-Waller correction to core and valence electrons separately, with B_{Li} and B_H thermal factors, respectively.

Table IV reports the observed and calculated structure factors for the two models; the MCS data are practically coincident with those obtained by Grosso and Pastori Parravicini[15] using the same model. The data have been

TABLE III. Energy data and valence-band eigenvalues for the MCS and EBS solutions.

	MCS	EBS
Total energy (a.u.)	−8.009 71	−8.062 89
Kinetic energy (a.u.)	8.081 65	8.067 73
Virial coefficient	1.004 5	1.000 3
Cohesive energy (a.u.)	0.283	0.338
Bulk modulus (dyn/cm^2)		3.41×10^{11}
Eigenvalues of the valence band at special $\vec{k}$ points (a.u.)		
Γ	−0.459 06	−0.492 19
X	−0.183 00	−0.247 25
W	−0.271 31	−0.249 66
L	−0.278 61	−0.388 33
K	−0.250 29	−0.265 81

TABLE IV. Calculated and observed x-ray structure factors. The reflections are labeled according to the usual criterion. For each of the two models the first two columns report the core and valence contributions to f_{hkl} without any thermal correction, while the data in the third and fourth columns are the $|f_{hkl}|$ after a Debye-Waller correction, with $B_H=1.8$ and B_{Li} as indicated. The agreement factors in the last row are calculated according to the formula $R=\sum|f_{hkl}^{expt}-f_{hkl}^{obs}|/\sum|f_{hkl}^{obs}|$. The thermal factors are in Å^2.

	MCS				EBS				
			Total corrected				Total corrected		
$h\,k\,l$	Core	Valence	$B_{Li}=1.01$	$B_{Li}=1.10$	Core	Valence	$B_{Li}=1.01$	$B_{Li}=1.10$	Observed
000	2.0	2.0	4.0	4.0	2.0	2.0	4.0	4.0	
111	−1.749	0.715	1.012	1.005	−1.734	0.681	1.029	1.022	1.086±0.002
200	1.676	0.534	2.057	2.048	1.658	0.510	2.018	2.010	2.032±0.003
220	1.425	0.239	1.454	1.441	1.440	0.233	1.427	1.414	1.454±0.004
311	−1.272	0.141	0.972	0.956	−1.247	0.148	0.946	0.930	0.960±0.004
222	1.227	0.138	1.123	1.107	1.201	0.142	1.104	1.088	1.096±0.002
400	1.068	0.091	0.897	0.879	1.044	0.098	0.883	0.865	0.888±0.002
331	−0.968	0.052	0.695	0.676	−0.946	0.062	0.672	0.654	0.671±0.005
420	0.938	0.066	0.732	0.713	0.916	0.072	0.719	0.701	0.738±0.002
422	0.830	0.050	0.603	0.585	0.812	0.056	0.594	0.576	0.600±0.003
333	−0.761	0.024	0.494	0.476	−0.745	0.033	0.479	0.462	0.472±0.006
511	−0.761	0.024	0.494	0.476	−0.745	0.033	0.479	0.462	0.474±0.004
440	0.663	0.033	0.422	0.405	0.652	0.037	0.417	0.400	0.414±0.003
531	−0.614	0.014	0.356	0.339	−0.604	0.020	0.347	0.331	0.354±0.001
442	0.598	0.028	0.358	0.341	0.590	0.031	0.354	0.338	0.349±0.001
600	0.598	0.028	0.358	0.341	0.590	0.031	0.354	0.338	0.359±0.002
620	0.542	0.025	0.304	0.289	0.536	0.026	0.302	0.286	0.299±0.001
533	−0.505	0.008	0.261	0.246	−0.501	0.013	0.257	0.242	0.248±0.002
622	0.494	0.022	0.261	0.246	0.490	0.023	0.259	0.245	0.250±0.001
441	0.451	0.019	0.223	0.210	0.450	0.020	0.223	0.209	0.209±0.002
551	−0.423	0.005	0.194	0.181	−0.422	0.009	0.193	0.180	0.182±0.003
711	−0.423	0.005	0.194	0.181	−0.422	0.009	0.193	0.180	0.179±0.001
R			0.024	0.019			0.018	0.029	

corrected with two sets of thermal factors taken from Calder's paper; for hydrogen, $B_H=1.80$ Å^2 was used in the two cases (resulting from neutron-scattering experiments); for lithium, the values $B_{Li}=1.01$ Å^2 (from x-ray scattering) and $B_{Li}=1.1$ Å^2 (an average between x-ray- and neutron-scattering determinations) were tried; the latter set has been adopted in previous theoretical work.[9(b),15] It is seen that the agreement between theory and experiment is generally satisfactory and that the theoretical data do not differ very much from each other. The quality of the agreement for high-index reflections, where the contribution from lithium is dominant, critically depends on the value of B_{Li}. The analysis of the low-index reflections, where thermal corrections are less important and qualitative differences in the description of valence electrons should come more easily to light, appears more interesting. It is precisely with the first reflection that the most marked disagreement between theory and experiment takes place. With respect to the observed (111) intensity, the MCS result is too low by about 8%, apparently because of an overestimation of the corresponding hydrogen structure factor. This has been taken as an indication of a partially covalent character of the Li—H bond[32] which cannot be accounted for by the MCS model. However, the EBS model does not seem to perform much better; it can be added that these results are relatively stable with respect to reasonable modifications of the basis set and thermal factors.

This large discrepancy between the experimental data and both theoretical results is perhaps to be attributed to insufficient accuracy of the experimental techniques. In the case of beryllium,[33–35] it has been shown lately that relatively recent[36] x-ray-diffraction data can be affected by systematic errors of the order of 6%.

A general conclusion can be drawn from the above discussion, namely, that the EBS and experimental charge-density data confirm by and large the ionic character of LiH. The covalent character of this crystal, if any, is very little; in fact, the Mulliken bond population between nearest neighbors, as obtained by the EBS calculation, is slightly negative (−0.005 electrons). The changes in charge distribution introduced by the EBS model with respect to the MCS model are most clearly described by directly referring to charge-density data. Table V reports the values of minimal charge density along the main three crystallographic directions, and the distance from hydrogen where it occurs. As expected, abandoning the strictly ionic model brings in a slight increase of density in the ionic interstices. The same features emerge more clearly from Fig. 1: The differential map $\rho_{EBS}-\rho_{MCS}$ on the (100) plane exhibits a flat relative maximum midway between next-nearest neighbors, revealing a smoother char-

TABLE V. Value and location of the minimum of the charge density along three crystallographic directions. d is the distance from hydrogen. ρ and d are expressed in a.u.

Direction	MCS		EBS	
	ρ	d	ρ	d
[100]	0.001 17	2.320	0.001 31	2.254
[110]	0.000 83	2.728	0.000 88	2.728
[111]	0.000 52	3.341	0.000 55	3.341

acter for the EBS charge density with respect to the MCS charge density, which finds a counterpart in the lower intensity of the first few valence structure factors.

D. Electron-momentum distribution

A very accurate set of experimentally determined CP's along five crystallographic directions of LiH have been recently produced by Reed.[37] The profiles have been corrected by removing the errors related to multiple-scattering events and to limited resolution; the corrected profiles are reported in Table I of Ref. 37 and will be referred to henceforth as Reed's experimental data. The information they contain is invaluable for discriminating between different theoretical models. In particular, as will be shortly demonstrated, the differential CP's at low momenta and the autocorrelation function $B(\vec{r})$ at intermediate distances (around 6 a.u.) are a subtle and reliable test of the accuracy of the theoretical description of the valence electrons of LiH. The EMD in the range 0—1.5 a.u. is, in fact, dominated by the contribution of the two valence electrons, and differences in the description of the valence wave function show up quite clearly here. This is shown in Fig. 2, which demonstrates the EMD along the main three crystallographic directions. It can first be observed that the use of an EBS appreciably reduces the value of the EMD at zero momentum, as is predictable on the basis of the virial theorem.[38] Regarding the anisotropy, the [100] curve is the most squarelike in shape in both cases, while the opposite is true for the [111] curve. This behavior is, however, much more evident in the EBS model, where there is a marked anisotropy also below 0.5 a.u.

A direct comparison of theoretical EMD data with experiment would require the reconstruction of the EMD from measured directional CP's. In order to avoid an accumulation of errors, it is, however, preferable to compare experimental with calculated CP's. Table VI reports the theoretical CP's for the two models along the five directions considered by Reed. The MCS results are very close to those obtained by Ameri *et al.*[16] with the same basis set using a 5GTO (instead of a 4GTO) approximation of the STO's, and are also less anisotropic than those reported by Aikala[11] who used, however, a slightly more expanded function for the hydride ion ($\alpha_H=0.7208$ a.u.). Figure 3 shows the four differential CP's, $J_{[100]}-J_{[ijk]}$; these quantities are particularly suitable for checking the quality of a calculated wave function because the differences between different theoretical models are evident, and also because many systematic errors which can affect the experimental CP's are canceled when subtracting one profile from the other. Along with the MCS and EBS data, here we have reported the differential CP's calculated by Ramirez *et al.*[39] following the method of the molecular simulated crystal, which had given satisfactory results with lithium fluoride.[40] We have not reported Aikala's[11] differential profiles since they closely resemble those obtained with the present MCS model, though slightly more anisotropic. From Fig. 3 it is seen that the EBS model gives the closest agreement with experiment, although it apparently un-

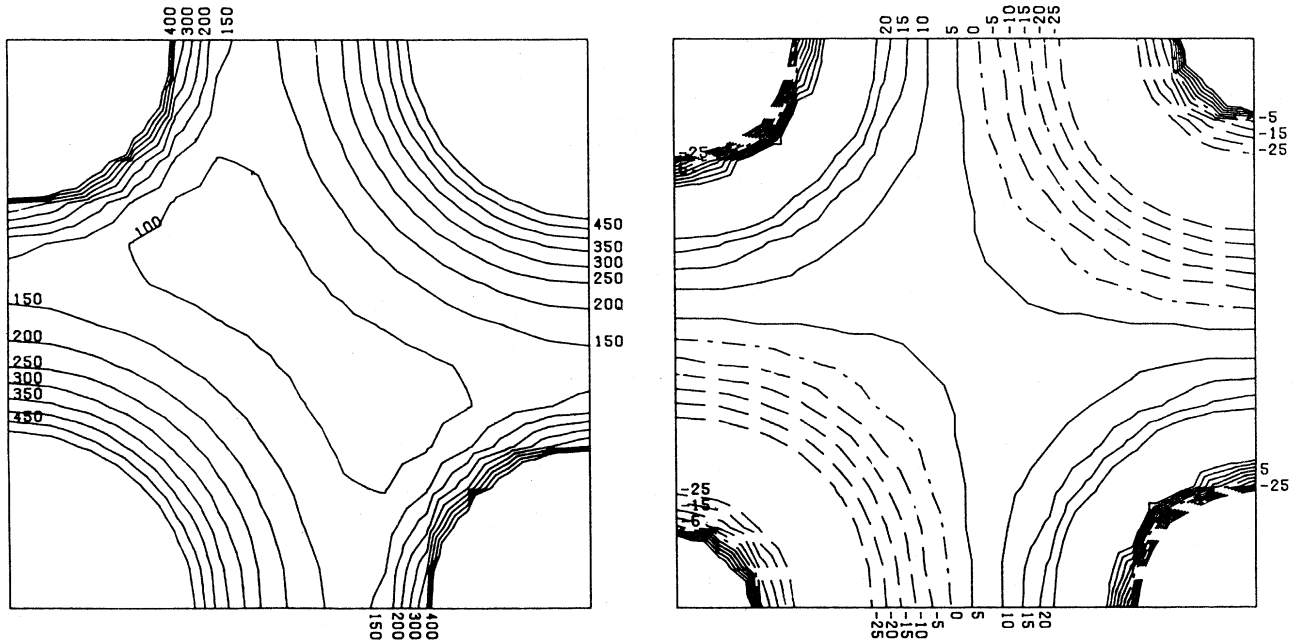

FIG. 1. Total charge density ρ_{EBS} (left) and differential charge density $\rho_{EBS}-\rho_{MCS}$ (right) on the (100) plane. The numbers on the isodensity lines are in units of 10^{-5} a.u.; the lithium atom is at the top left and bottom right in each plot.

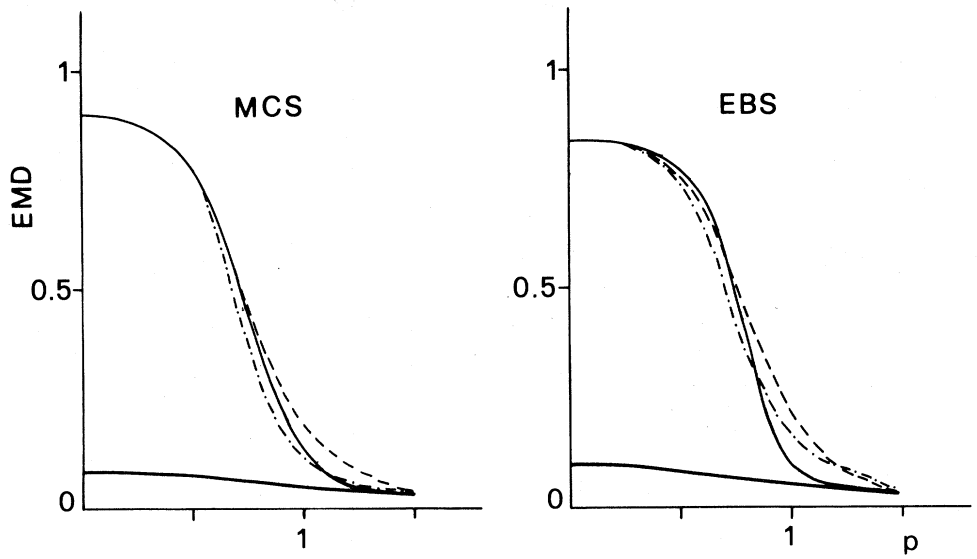

FIG. 2. Calculated EMD along three crystallographic directions for the two models. Different lines refer to different directions as follows: solid line, [100]; dashed line, [110]; dotted-dashed line, [111]. The heavy solid line is the contribution from core electrons. Here and in the following figures a.u. are used throughout.

derestimates anisotropies; we will return to this point. The data by Ramirez are furthest from experiment; interestingly enough, as pointed out by Reed, the experimental maxima, minima, and zeros (confirmed by the EBS model) are located at positions which are generally intermediate between the fully ionic model (MCS) and the molecular-simulated-crystal model of Ramirez *et al.*, which exaggerates the covalent character of the Li—H bond. Owing to the preceding discussion on the structure factors, one must be very careful in interpreting this

TABLE VI. Directional CP's obtained with the MCS and EBS solutions.

	[100]		[110]		[111]		[112]		[221]	
	MCS	EBS	MCS	EBS	MCS	EBS	MCS	EBS	MCS	EBS
0.0	2.259	2.243	2.182	2.219	2.273	2.294	2.260	2.271	2.235	2.255
0.1	2.221	2.201	2.159	2.193	2.237	2.259	2.220	2.234	2.210	2.240
0.2	2.116	2.095	2.102	2.131	2.137	2.160	2.121	2.141	2.128	2.156
0.3	1.956	1.956	2.007	2.031	1.978	2.006	1.973	2.001	1.994	2.015
0.4	1.757	1.795	1.833	1.853	1.773	1.805	1.787	1.823	1.802	1.829
0.5	1.536	1.614	1.600	1.616	1.544	1.578	1.565	1.604	1.571	1.603
0.6	1.312	1.410	1.337	1.351	1.304	1.333	1.318	1.351	1.315	1.338
0.7	1.099	1.180	1.070	1.081	1.070	1.086	1.075	1.095	1.069	1.084
0.8	0.907	0.940	0.862	0.870	0.867	0.869	0.866	0.871	0.859	0.864
0.9	0.745	0.731	0.697	0.700	0.710	0.701	0.705	0.699	0.700	0.695
1.0	0.616	0.580	0.581	0.578	0.594	0.581	0.590	0.577	0.586	0.576
1.1	0.517	0.478	0.504	0.496	0.509	0.494	0.508	0.492	0.504	0.492
1.2	0.442	0.407	0.442	0.429	0.442	0.427	0.444	0.427	0.441	0.427
1.3	0.383	0.356	0.391	0.375	0.388	0.373	0.392	0.375	0.391	0.376
1.4	0.337	0.316	0.350	0.333	0.344	0.331	0.347	0.332	0.348	0.332
1.5	0.300	0.284	0.313	0.296	0.308	0.296	0.309	0.295	0.310	0.296
1.6	0.268	0.255	0.279	0.264	0.276	0.265	0.276	0.263	0.277	0.264
1.7	0.240	0.230	0.248	0.236	0.248	0.237	0.247	0.236	0.248	0.236
1.8	0.216	0.207	0.222	0.211	0.223	0.212	0.221	0.211	0.222	0.211
1.9	0.194	0.187	0.198	0.189	0.199	0.189	0.197	0.188	0.198	0.189
2.0	0.175	0.169	0.176	0.169	0.177	0.168	0.176	0.168	0.177	0.168
2.5	0.102	0.098	0.101	0.096	0.100	0.095	0.100	0.095	0.100	0.095
3.0	0.057	0.054	0.057	0.055	0.057	0.055	0.057	0.055	0.057	0.055
3.5	0.033	0.032	0.033	0.032	0.033	0.032	0.033	0.032	0.033	0.032
4.0	0.020	0.019	0.020	0.019	0.020	0.019	0.020	0.019	0.020	0.019
5.0	0.007	0.008	0.007	0.008	0.007	0.008	0.007	0.008	0.007	0.008
6.0	0.003	0.003	0.003	0.003	0.003	0.003	0.003	0.003	0.003	0.003
7.0	0.001	0.001	0.001	0.001	0.001	0.001	0.001	0.001	0.001	0.001

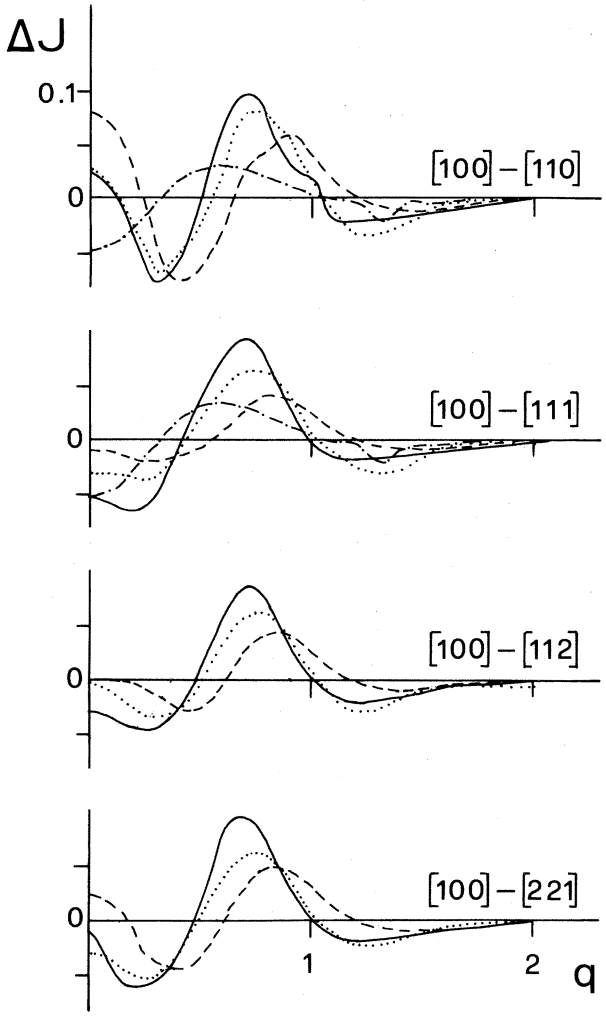

FIG. 3. Differential CP's $J_{[100]}(q)-J_{[ijk]}(q)$, as indicated. The different lines refer to different cases as follows: solid line, EBS calculation; dashed line, MCS calculation; dotted-dashed line, Ramirez *et al.* calculation (Ref. 39); dotted line, experimental data (Ref. 37).

feature as an indication of a partially covalent character of the Li—H bond. Rather, it can be observed that the analysis of the CP's can provide higher discriminating power between different theoretical models with respect to more traditional x-ray-diffraction data. The Fourier transform of CP's, the so-called autocorrelation function $B(\vec{r})$, provides an important check of the quality of individual directional CP's. The main features of these functions can be summarized as follows.[41–43]

(a) Their value at $r=0$ must equal the number N of electrons; this allows a check of the accuracy of the adopted numerical techniques.

(b) In periodic systems, the sign of $B(\vec{r})$ is typically alternating over distances which are of the order of magnitude of the lattice parameter. More precisely, when considering nonconducting systems, the autocorrelation function along a given direction is bound to be zero at $\vec{r}$ values which are a multiple of the fundamental translation distance $\vec{r}_{ijk}$ along that direction. Verifying how precisely

TABLE VII. Zero passages (in a.u.) of the autocorrelation function along different directions for the two theoretical models considered and for Reed's experimental (expt.) results (Ref. 37); the last column gives the reticular zero passages imposed by symmetry (geom. for geometrical).

	MCS	EBS	Expt.	Geom.
[100]	6.68	5.14	5.25	
	7.73	7.72	7.80	7.72
	12.20	12.78	11.08	
[110]	5.45	5.45	5.44	5.46
	10.93	10.92	13.07	10.91
	16.16	16.29		16.37
[111]	6.18	5.87	5.70	
	9.56	9.34	8.70	
	13.25	13.38	10.63	13.36
[112]	5.89	5.62	5.54	
	9.45	9.45	9.36	9.45
	15.25	14.85	11.25	
[221]	5.77	5.65	5.57	
	10.37	10.13	9.70	
	14.56	14.00	11.07	

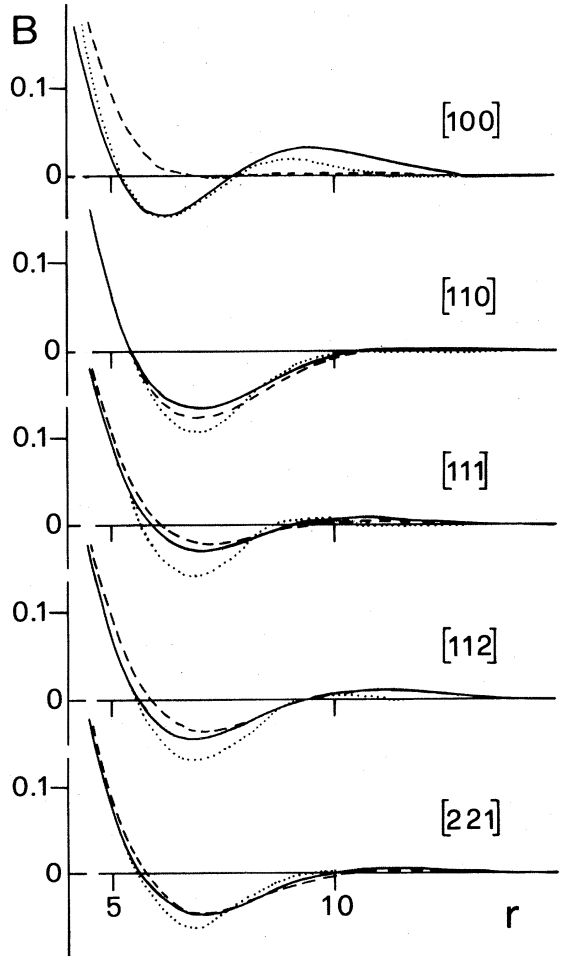

FIG. 4. Autocorrelation function $B(\vec{r})$ along different directions. The symbols adopted are as in Fig. 3.

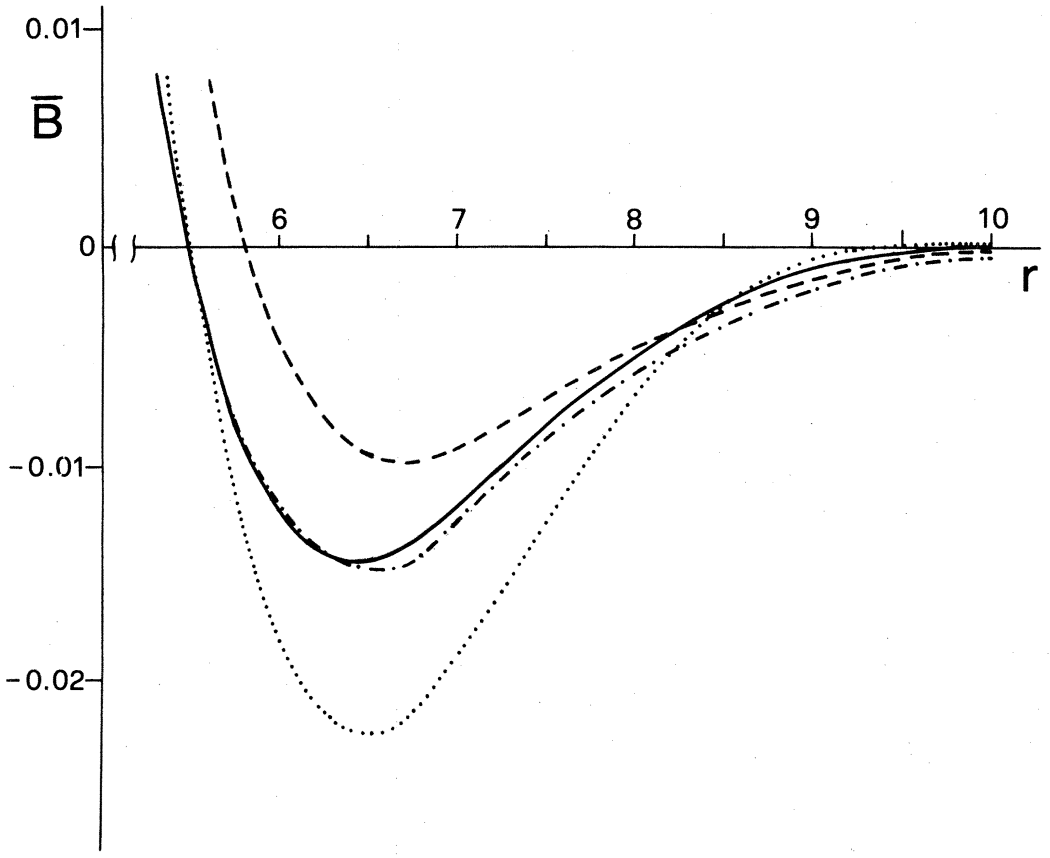

FIG. 5. Average autocorrelation function $\bar{B}(r)$ with damping factor included (see text). The dotted-dashed curve refers to the experimental data of Pattison and Weyrich (Ref. 17); the other symbols are as in Fig. 3.

these "reticular zero passages" are reproduced not only permits us to evaluate the formal correctness of the calculated wave functions (in particular concerning the orthogonality constraint), but also provides a satisfactory test of the range of reliability of experimental data.

(c) The experimental error has been shown to affect $B(\vec{r})$ essentially as a damping factor $D(\vec{r})=\exp(-\beta^2 r^2)$, where β is proportional to the resolution in momentum space.

Table VII reports the location of the first reticular and nonreticular zero passages for Reed's data, and for the two theoretical calculations. A more detailed description of the behavior of the experimental and theoretical autocorrelation functions around the first minimum is provided by Fig. 4. The first observation that applies to those data is that the first reticular zeros are well accounted for by all theoretical calculations, while Reed's data satisfactorily reproduce the zero locations up to $r\sim 10$ a.u., but do not clearly identify subsequent zeros. This suggests that a comparison with experimental data is meaningful up to about that distance, which is, however, sufficient for discriminating between the theoretical calculations in favor of the EBS model. Figure 4 shows that the calculation performed with the extended set also provides semiquantitative agreement with Reed's data concerning the position and values of relative maxima and minima. The most important disagreement encountered between Reed's and EBS data concerns the entity of $B(\vec{r})$ at the minimum, which appears somewhat underestimated by the theoretical calculation. The same effect could, however, be attributed to an overcorrection of experimental data for limited resolution.

In order to check this point, we report in Fig. 5 the experimental average autocorrelation function $\bar{B}(r)$, obtained by Pattison and Weyrich[17] with a polycrystalline sample, along with the corresponding theoretical curves calculated according to the two models and multiplied by the experimental damping factor $D(r)$. For comparison, $\bar{B}(r)$ is also reported obtained from Reed's data according to the following procedure: An average CP has first been obtained as a weighted average of Reed's directional CP's; after Fourier transformation the resulting values have been corrected using Pattison's damping factor. The following observations apply to the data reported in Fig. 5. (a) We believe that the curve by Pattison and Weyrich is particularly reliable and can be taken as a reference because of the simplicity of their experimental setup and of the very high peak-to-background ratio. (b) The first zero practically coincides for the two experimental curves and for the EBS curve, while it is clearly offset with the MCS model. (c) Reed's minimum is much lower than Pattison's, probably to indicate that Reed's data for the minimum are overcorrected by the author himself. (d) On the contrary, Reed's curve is much nearer to the zero line with respect to Pattison's beyond 9 a.u. Perhaps the last two observations are indicative of some deficiency in Reed's procedure

for correcting the CP's for experimental errors; clearly, if Reed's directional $B(\vec{r})$'s were renormalized in order to bring their average in accordance with Pattison's $\bar{B}(r)$, their agreement with the EBS data would become much closer.

IV. CONCLUSIONS

A quite complete *ab initio* study of crystalline LiH at a HF level of approximation has here been presented. The use of a very large basis set, able to describe the polarizability properties of the hydride ion, has been made possible by an accurate treatment of Coulomb interactions up to infinite distance. The results are, in general, in good agreement with experiment. With respect to minimal-basis-set calculations, there are definite improvements in the evaluation of the cohesive energy and in the description of the electron-momentum distribution, while x-ray-diffraction data do not discriminate between the two models. On the whole, the EBS calculation confirms the hypothesis of substantially ionic character of crystalline LiH.

The application of the present computational scheme to other ionic systems is in progress. We do not expect to meet particular difficulties in their treatment: Although the study of LiH is made easier by its having only four electrons per unit cell, the accurate treatment of the large and extremely polarizable hydride ion is certainly a severe test of the computational techniques.

ACKNOWLEDGMENTS

The authors want to thank Dr. Vic Saunders for valuable discussions, and the Italian Ministero della Pubblica Istruzione for financial support.

[1]J. L. Calais, Int. J. Quantum Chem. Symp. 9, 497 (1975).
[2]E. A. Hylleraas, Z. Phys. 63, 771 (1930).
[3]S. O. Lundqvist, Ark. Fys. 8, 177 (1954).
[4]I. Waller and S. O. Lundqvist, Ark. Fys. 7, 121 (1953).
[5]A. Westin, I. Waller, and S. O. Lundqvist, Ark. Fys. 22, 371 (1962).
[6]A. B. Kunz, Phys. Status Solidi. 36, 301 (1969).
[7]A. B. Kunz, Phys. Rev. B 6, 3019 (1972).
[8]K. F. Berggren and F. Martino, Phys. Rev. B 3, 1509 (1971).
[9](a) J. Felsteiner, R. Fox, and S. Kahane, Phys. Rev. B 6, 4689 (1972); (b) S. Kahane, J. Felsteiner, and R. Opher, Phys. Rev. B 8, 4875 (1973).
[10]A. B. Kunz and D. J. Mickish, Phys. Rev. B 11, 1700 (1983).
[11]O. Aikala, J. Phys. C 9, L131 (1976).
[12]T. Paakkari, V. Halonen, and O. Aikala, Phys. Rev. B 13, 4602 (1976).
[13]G. Grosso, G. Pastori Parravicini, and R. Resta, Phys. Status Solidi B 73, 371 (1976).
[14]G. Grosso and G. Pastori Parravicini, J. Phys. C 10, L451 (1977).
[15]G. Grosso and G. Pastori Parravicini, Phys. Rev. B 17, 3421 (1978).
[16]S. Ameri, G. Grosso, and G. Pastori Parravicini, Phys. Rev. B 23, 4242 (1981).
[17]P. Pattison and W. Weyrich, J. Phys. Chem. Solids 40, 213 (1979).
[18]R. Bauer, J. Nonmetals 1, 257 (1973).
[19]C. Pisani and R. Dovesi, Int. J. Quantum Chem. 17, 501 (1980).
[20]R. Dovesi, C. Pisani, C. Roetti, and V. R. Saunders, Phys. Rev. B 28, 5781 (1983).
[21]R. Dovesi, C. Pisani, C. Roetti, and P. Dellarole, Phys. Rev. B 24, 4170 (1981).
[22]P. P. Ewald, Ann. Phys. (N.Y.) 4, 64, 253 (1921).
[23]M. Tosi, in *Solid State Physics,* edited by F. Seitz and D. Turnbull (Academic, New York, 1964), Vol. 16, p. 1.
[24]F. E. Harris, in *Theoretical Chemistry Advances and Perspectives,* edited by H. Eyring and D. Henderson (Academic, London, 1975), Vol. 1, p. 147.
[25]W. J. Hehre, R. F. Stewart, and J. A. Pople, J. Chem. Phys. 51, 2657 (1969).
[26]R. P. Hurst, Phys. Rev. 114, 746 (1959).
[27]R. Dovesi, E. Ferrero, C. Pisani, and C. Roetti, Z. Phys. B 51, 195 (1983).
[28]E. Clementi and C. Roetti, At. Data Nucl. Data Tables 14, 177 (1974).
[29]C. R. Fischer, T. A. Dellin, S. W. Harrison, R. D. Hatcher, and W. D. Wilson, Phys. Rev. B 1, 876 (1970).
[30]G. T. Surratt, R. N. Euwema, and D. L. Wilhite, Phys. Rev. B 8, 4019 (1973).
[31]G. Grosso and G. Pastori Parravicini, Phys. Rev. B 20, 2366 (1979).
[32]R. S. Calder, W. Cochran, D. Griffiths, and R. D. Lowde, J. Phys. Chem. Solids 23, 621 (1962).
[33]N. K. Hansen, J. R. Schneider, and F. K. Larsen (unpublished).
[34]F. K. Larsen and N. K. Hansen (private communication).
[35]R. Dovesi, C. Pisani, F. Ricca, and C. Roetti, Phys. Rev. B 25, 3731 (1982).
[36]P. T. Brown, Philos. Mag. 26, 1377 (1972).
[37]W. A. Reed, Phys. Rev. B 18, 1986 (1978).
[38]I. R. Epstein and A. C. Tanner, in *Compton Scattering,* edited by B. Williams (McGraw-Hill, New York, 1977).
[39]B. I. Ramirez, W. R. McIntire, and R. L. Matcha, J. Chem. Phys. 66, 373 (1977).
[40]B. I. Ramirez, W. R. McIntire, and R. L. Matcha, J. Chem. Phys. 65, 906 (1976).
[41]P. Pattison and W. Weyrich, Solid State Commun. 20, 585 (1976).
[42]B. Kramer, P. Krusius, W. Schroeder, and W. Schülke, Phys. Rev. Lett. 38, 1227 (1977).
[43]P. Pattison, W. Weyrich, and B. Williams, Solid State Commun. 21, 967 (1977).